ACCSCIENCE PUBLISHING

Journal of Seismic Exploration

ARTICLE

Microseismic event locations using grid-searching method and Newton–Raphson-based optimizer

Shaohui Zhou[1], Tianqi Jiang[2]*, Junhao Qu[1], Peng Lin[2], Yu Wang[1], and Yajun Li[1]

[1]Shandong Earthquake Agency, Jinan, Shandong, China

[2]State Key Laboratory for Fine Exploration and Intelligent Development of Coal Research, China University of Mining and Technology-Beijing, Beijing, China

(This article belongs to the *Special Issue: Advanced Artificial Intelligence Theories and Methods for Seismic Exploration*)

Abstract

Microseismic event location plays a pivotal role in industrial applications, such as coal mining and hydraulic fracturing, by revealing subsurface fracture dynamics through the spatiotemporal analysis of seismic events. As a cornerstone of microseismic monitoring, accurate event localization enables critical insights into underground structural integrity. Traditional arrival-time-based methods employ optimization algorithms to minimize residuals between observed and theoretical arrival times. While this classical approach has proven effective, its accuracy is often compromised by two key limitations: suboptimal initial iteration values and inaccuracies in velocity parameter estimation. To address these challenges, we propose an innovative localization method integrating a grid-searching strategy with a Newton–Raphson-based optimizer. Our approach begins by generating initial iterative vectors—comprising event coordinates and velocity parameters—through a systematic grid-searching technique. Subsequently, the Newton–Raphson optimizer refines these estimates within a four-dimensional search space to achieve high-precision inversion results. The efficacy of the proposed method was rigorously evaluated using both synthetic and field datasets, with comparative analyses conducted against four established localization techniques. Experimental results demonstrate that our method significantly enhances localization accuracy and robustness, reliably inverting both event locations and velocity parameters. These findings provide a valuable technical reference for advancing microseismic monitoring systems, offering improved precision in industrial applications.

Keywords: Microseismic event location; Grid-searching method; Newton–Raphson-based optimizer

***Corresponding author:**
Tianqi Jiang
(jiang_tianqi0623@163.com)

Citation: Zhou S, Jiang T, Qu J, Lin P, Wang Y, Li Y. Microseismic event locations using grid-searching method and Newton–Raphson-based optimizer. *J Seismic Explor*. 2025;34(2):60-71.
doi: 10.36922/JSE025320052

Received: August 04, 2025

Revised: August 22, 2025

Accepted: September 02, 2025

Published online: September 11, 2025

1. Introduction

Microseismic monitoring has gained significant attention across multiple disciplines including mining engineering,[1] carbon capture and utilization,[2] volcanic activity

monitoring,[3] and hydrocarbon reservoir characterization.[4] The accuracy and reliability of microseismic event localization are paramount in these applications, as the methodology must maintain robustness and stability when processing potentially noise-contaminated datasets.

Current localization approaches typically utilize the residuals between theoretical and observed P-wave arrival times as the primary criterion for evaluating inversion quality. The standard workflow involves: (i) identifying actual P-wave arrivals from recorded waveforms, (ii) implementing optimization algorithms to iteratively determine the spatial coordinates that minimize the discrepancy between calculated and observed travel times.

Time-based localization methods, which rely on arrival time picking, ray tracing, primarily originate from the classical Geiger algorithm.[5] These methods determine the source location by identifying the spatial coordinates that minimize the residuals between observed first-arrival times and theoretical travel times.[6,7] However, the accuracy of such localization results is fundamentally constrained by inherent limitations in velocity model accuracy,[8-11] often leading to suboptimal positioning performance. To address these challenges, recent research efforts have focused on two key aspects: (1) developing enhanced optimization algorithms[12,13] and (2) optimizing sensor array configurations.[14-17]

The integration of multiple optimization methods has proven to be an effective strategy for enhancing the accuracy of microseismic event localization. Several hybrid approaches have demonstrated promising results: Jiang and Pei.[18] developed a combined grid search and Newton–Raphson iteration method; Lü *et al.*[19] implemented a hybrid algorithm incorporating simulated annealing with the simplex method; and Luo *et al.*[20] proposed a novel approach utilizing seagull optimization combined with quantile difference analysis. These hybrid methods have shown significant improvements in localization accuracy compared to conventional single-algorithm approaches.

However, the velocity model remains a critical factor affecting localization precision. Dong *et al.*[21] addressed this challenge by developing a velocity-independent localization method that eliminates the need for pre-measured velocity parameters. While this approach effectively mitigates velocity related errors, it inherently lacks the capability to simultaneously invert for velocity parameters during the localization process.

We present a novel microseismic event localization method that combines the grid searching rule with a Newton-Raphson-based optimizer (GNRBO). Unlike conventional Newton-Raphson implementations that employ random initial assignments, our approach systematically generates initial iterative vectors (comprising both event coordinates and velocity parameters) through comprehensive grid sampling. The Newton-Raphson optimizer then refines these estimates within a four-dimensional parameter space, simultaneously solving for both the microseismic source location and the average velocity model.

To evaluate the method's performance, we conducted extensive testing using both synthetic and field datasets, assessing the algorithm's accuracy and stability under various conditions. For comparative analysis, we implemented three established optimization techniques: the Hooke-Jeeves (H-J) direct search method, Genetic Algorithm (GA), and Particle Swarm Optimization (PSO). Results demonstrate that our proposed GNRBO method outperforms these benchmark approaches in both localization accuracy and computational stability.

2. Methods

2.1. Target function

Time-based microseismic localization methods utilize the minimization of residuals between theoretical and observed arrival times as their fundamental principle. Through optimization algorithms, these methods systematically search the potential source space to identify spatial coordinates where the travel-time residuals satisfy predetermined convergence criteria. The source location is considered accurately determined when the minimized residuals achieve the required inversion precision threshold.

The theoretical arrival time of microseismic waves at geophones can be expressed as a function of three key parameters as follows: (1) the spatial coordinates of the seismic source, (2) the receiver positions, and (3) the velocity model of underground wave propagation. This fundamental relationship forms the basis for time-based localization methods and can be mathematically described as follows:

$$T_P^i\left(x_0, y_0, z_0, v_0, T_0\right) = T_0 + t_P^i\left(x_0, y_0, z_0, v_0\right) \quad \text{(I)}$$

Where T_P^i denotes the observed P-wave arrival time at the i-th receiver (**Equation I**), and T_0 represents the origin time of the event.

t_P^i (**Equation II**) corresponds to the theoretical P-travel time from the location (x_0, y_0, z_0) to the i-th receiver at (X_i, Y_i, Z_i) and the velocity parameter is v_0:

$$t_P^i = \sqrt{\frac{\left(X_i - x_0\right)^2 + \left(Y_i - y_0\right)^2 + \left(Z_i - z_0\right)^2}{v_0}} \quad \text{(II)}$$

After eliminating the origin time T_0, the inversion problem reduces to four unknown parameters in the objective function $R(x,y,z,v)$, namely the source coordinates $R(x,y,z)$ and the effective P-wave velocity (v_0). This function quantifies the travel-time residuals between observed and theoretical arrivals as follows:

$$R\left(x,y,z,v\right) = \sqrt{\frac{1}{N}\sum_{i=1}^{N}\left(T_p^i\left(x,y,z,v\right) - T_p^i\left(x_0,y_0,z_0,v_0\right)\right)^2} \quad \text{(III)}$$

$T_p^i\left(x,y,z,v\right)$ is the theoretical P-arrival time:

$$T_p^i\left(x,y,z,v\right) = \hat{T}_0 + t_P^i\left(x,y,z,v\right) \quad \text{(IV)}$$

$\hat{T}_0$ is the estimate of the origin time of the event:

$$\hat{T}_0 = \frac{1}{N}\sum_{i=1}^{N}\left(T_p^i\left(x_0,y_0,z_0,v_0\right) - t_P^i\left(x,y,z,v\right)\right) \quad \text{(V)}$$

According to **Equation III**, when the inversion unknowns approach the true value, the target function value is smaller. Inversions based on the location and velocity of the microseismic event are process in which the optimization algorithm is used to solve the unknowns of the target function, so that the target function tends to 0 and achieves the global optimum.

As shown in **Equation III**, the objective function exhibits an inverse relationship with parameter accuracy, achieving its minimum value when the inverted parameters converge to their true values. The inversion process for microseismic event location and velocity determination constitutes an optimization problem where the algorithm iteratively adjusts the unknown parameters (x,y,z,v) to the minimization of the objective function toward zero.

2.2. Grid-searching method

The grid-search method systematically discretizes the parameter space to generate initial candidate solutions and establishes a set of potential solutions through a rough spatial sampling for the subsequent Newton-Raphson optimization. The searching rule is defined as:

$$\begin{cases} x_i = x_{min} + i\Delta x, & \left(i = 0,1,...,nx\right) \\ y_j = y_{min} + j\Delta y, & \left(j = 0,1,...,ny\right) \\ z_k = z_{min} + k\Delta z, & \left(k = 0,1,...,nz\right) \\ v_l = v_{min} + l\Delta v, & \left(l = 0,1,...,nv\right) \end{cases} \quad \text{(VI)}$$

Where (x_{min}, y_{min}, z_{min}, v_{min}) is the lower bounds in the searching space and (Δx, Δy, Δz, Δv) specifying the discrete interval between adjacent grid points along each axis. nx, ny, nz and nv are sampling numbers in each axis.

We define the swarms in the searching space as:

$$X_{n(i,j,k,l)} = \left(x_i, y_j, z_k, v_l\right) \quad \text{(VII)}$$

According to **Equation VII**, there are $N = nx \times ny \times nz \times nv$ vectors (swarms in the searching space). The initial iteration vectors then are used for Newton-Raphson searching rule in the next section.

2.3. Newton-Raphson searching rule

The Newton-Raphson searching rule is:

$$NRSR = randn \times \frac{\left(X_w - X_b\right) \times \Delta x}{2 \times \left(X_w + X_b - 2 \times X_n\right)} \quad \text{(VIII)}$$

randn is a normally distributed random number with zero mean, and unit variance; X_w is the worst performing solution vector (maximum objective function value); X_b is the best performing solution vector (minimum objective function value); X_n is the n-th generation of the searching swarm population.

The iteration rule is:

$$X_n^{IT+1} = X_n^{IT} - NRSR \quad \text{(IX)}$$

X_n^{IT} represents the n-th generation of the swarm population.

According to Sowmya *et al.*,[22] the iteration rule can be optimized further as:

$$\begin{cases} NRSR = randn \times \dfrac{\left(y_w - y_b\right) \times \Delta x}{2 \times \left(y_w + y_b - 2 \times X_n\right)} \\ y_w = r_1 \times \left(Mean\left(Z_{N+1} + x_n\right) + r_1 \times \Delta x\right) \\ y_b = r_1 \times \left(Mean\left(Z_{N+1} + x_n\right) - r_1 \times \Delta x\right) \\ Z_{n+1} = x_n - randn \times \dfrac{\left(X_w - X_b\right) \times \Delta x}{2 \times \left(X_w + X_b - 2 \times X_n\right)} \\ \Delta x = rand\left(1, dim\right) \times \left|X_n - X_n^{IT}\right| \end{cases} \quad \text{(X)}$$

Where r_1 denotes a uniformly distributed random variable on the interval (0,1), and *rand*(*1*, *dim*) represents a *dim*-dimensional random vector with components independently drawn from U(0,1). The updated iterative scheme is then given by:

$$\begin{cases} X_n^{IT+1} = r_2 \times \left(r_2 \times X1_n^{IT} + \left(1 - r_2\right) \times X2_n^{IT} + \right) + \left(1 - r_2 \times X3_n^{IT}\right) \\ X1_n^{IT} = X_n^{IT} - NRSR + \rho \\ X2_n^{IT} = X_b - NRSR + \rho \\ X3_n^{IT} = X_n^{IT} - \delta \times \left(X2_n^{IT} - X1_n^{IT} \right) \\ \rho = a \times \left(X_b - X_n^{IT} \right) + b \times \left(X_{t1}^{IT} - X_{t2}^{IT} \right) \\ \delta = \left(1 - \left(\dfrac{2 \times IT}{MAX\_IT} \right) \right)^5 \end{cases} \quad \text{(XI)}$$

Where a and b are random values in (0,1), $t1$ and $t2$ are random integers in the range of the number of iteration vector N. MAX_IT is the maximum generation number of the searching swarm population.

To enhance the robustness of the optimization process and prevent premature convergence to local optima, a Trap Avoidance Operator (TAO) is considered to dynamically evaluate and adjust the iteration vectors. This mechanism operates as follows:

$$\begin{cases} X_{TAO}^{IT} = X_n^{IT+1} + \theta_1 \times \left(\mu_1 \times X_b - \mu_2 \times X_n^{IT} \right) + \theta_2 \times \delta \times \\ \left(\mu_1 \times mean\left(X^{IT} - \mu_2 \times X_n^{IT} \right) \right), \mu_1 < 0.5 \\ X_{TAO}^{IT} = X_b + \theta_1 \times \left(\mu_1 \times X_b - \mu_2 \times X_n^{IT} \right) + \theta_2 \times \delta \times \\ \left(\mu_1 \times mean\left(X^{IT} - \mu_2 \times X_n^{IT} \right) \right), \mu_1 \geq 0.5 \end{cases} \quad \text{(XII)}$$

Where θ_1 is a random value in (−1,1), θ_2 is a random value in (−0.5,0.5), while μ_1 and μ_2 are represented by:

$$\begin{cases} \mu_1 = \beta \times 3 \times rand + \left(1 - \beta\right) \\ \mu_2 = \beta \times rand + \left(1 - \beta\right) \end{cases} \quad \text{(XIII)}$$

During the iteration, if the random number is less than the decision factor (DF, which is 0.6 in this paper), the particles are updated so that:

$$X_n^{IT+1} = X_{TAO}^{IT} \quad \text{(XIV)}$$

According to Sowmya *et al.*,[22] β denotes a binary number, either 1 or 0. If the value of a random value between 0 and 1 is ≥0.5, then the value of β is 0; otherwise, the value is 1. We assume that the optimization algorithm obtains the best performing solution when the iteration process is finished. Figure 1 illustrates the workflow of the proposed approach to visualize the key steps.

3. Synthetic data tests

The numerical simulation establishes a three-dimensional monitoring volume spanning *1000m* (*x-axis*) × *1000m* (*y-axis*) × *500m* (*z-axis*). The sensor network consists of eight seismic receivers (blue rectangular markers) deployed underground, while 10 synthetic microseismic sources (red spherical markers) are distributed throughout the volume to test localization performance (Figure 2).

The coordinates of the sensors and events, along with the average velocity of the monitoring area and the origin times of events, are presented in Tables 1 and 2.

To evaluate the performance of the proposed method in terms of positioning accuracy and convergence stability, we conducted tests using simulated P-wave travel times. For comparison, three established algorithms—the H-J

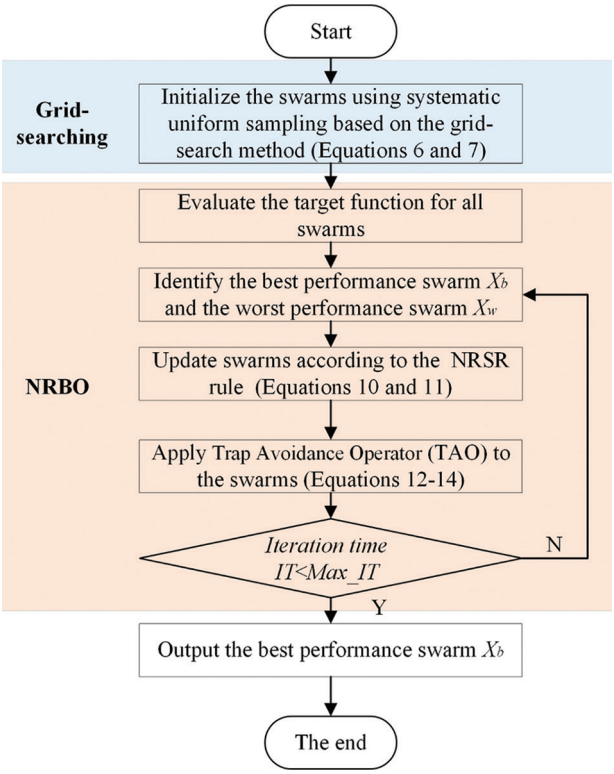

Figure 1. The flowchart of the proposed method. Abbreviations: NRBO: Newton–Raphson-based optimizer; NRSR: Newton–Raphson Search Rule.

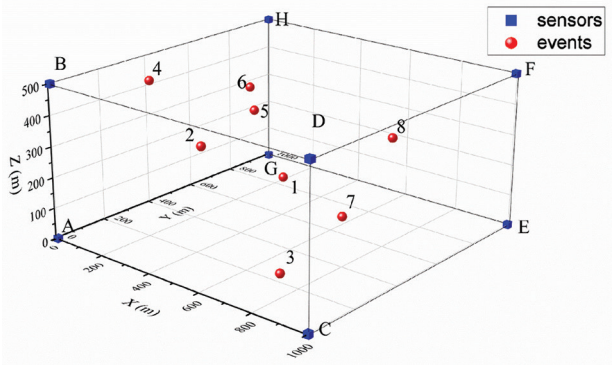

Figure 2. Sensor arrays and distribution of microseismic events.

algorithm, GA, PSO, and NRB)—were selected and benchmarked against the proposed approach.

3.1. Inversion results analysis on a single event

To evaluate the localization performance, synthetic P-wave arrival times were used, with each positioning method tested 10 times under identical conditions. For the H-J algorithm, 10 random initial values were generated per trial to assess robustness. The iteration parameters for the GA, PSO, NRBO, and the proposed method are detailed in Table 3.

Table 1. Coordinates of sensors in the monitoring area

Sensor	Coordinates of the sensors (m)		
	X	Y	Z
A	0	0	0
B	0	0	500
C	1000	0	0
D	1000	0	500
E	1000	1000	0
F	1000	1000	500
G	0	1000	0
H	0	1000	500

Table 2. Microseismic event locations and average velocities

Event	Event locations (m)			Velocity model (m/ms)	Origin time (ms)
	X	Y	Z	V	T_0
1	409	595	132	5	200
2	263	603	401	5	200
3	712	222	15	4.5	300
4	118	297	465	4.5	300
5	439	186	354	5.2	400
6	381	489	377	5.2	400
7	765	445	138	4.8	500
8	796	646	339	4.8	500

As shown in Table 4, the location errors and velocity inversion errors were evaluated based on the residual values of the objective function for each method. The results demonstrate that the PSO, NRBO, and the proposed method achieve higher positioning accuracy compared to the H-J algorithm and GA. The inversion results reveal that although the H-J algorithm converges close to the actual source location and approximates the average velocity in most cases, its solution often fails to reach the global optimum due to sensitivity to initial values, so the H-J method's positioning accuracy is significantly influenced by the selection of initial iteration points.

Furthermore, we observed that GNRBO achieves the same localization accuracy as NRBO. The proposed method employs a grid-search strategy for initial vector assignment instead of the random initialization used in NRBO. This approach is motivated by the fact that completely random initialization may concentrate all initial individuals in an unfavorable region of the search space. If this region is distant from the global optimum, the algorithm would require more time to explore other promising areas. In contrast, grid search ensures a uniform distribution of the initial population across the entire search space. As a result, GNRBO maintains the location accuracy of NRBO while mitigating the effects of random vector initialization. Given the near-identical characteristics of the two methods, the remainder of this paper discusses the performance of GNRBO only.

To evaluate the inversion accuracy and stability of the four comparison methods, we analyzed the residual curves of their objective functions (Figure 3). The results demonstrate that both the PSO method and the proposed method achieve superior localization accuracy compared to the other two approaches. Furthermore, both the H-J algorithm and PSO demonstrate susceptibility to local optima convergence. While the GA avoids this pitfall, its overall convergence performance remains suboptimal. Consequently, all three methods exhibit large standard deviations in their inversion results, indicating unsatisfactory stability in solution quality. As

Table 3. Iteration parameters of three algorithms for comparison

Method	The range of the searching spaces				Numbers of iteration vectors	Maximum number of iterations
	X (m)	Y (m)	Z (m)	Velocity (m/ms)		
GA	[0,1000]	[0,1000]	[0,500]	[3,7]	1000	500
PSO	[0,1300]	[0,1300]	[0,700]	[2,7]	144	500
NRBO	[0,1300]	[0,1300]	[0,700]	[2,7]	144	500
GNRBO	[−100,1300]	[−100,1300]	[−200,700]	[2,7]	144 (nx=ny=4; nz=nv=3)	500

Abbreviations: GA: Genetic Algorithm; GNRBO: Grid searching rule with an NRBO; PSO: Particle Swarm Optimization; NRBO: Newton-Raphson-based optimizer.

Table 4. Inversion results of each algorithm for No. 3 event

Method	No.	Inversion results				
		Values of target functions	Errors on X-axis (m)	Errors on Y-axis (m)	Errors on Z-axis (m)	Velocity error (m/ms)
H-J	1	1.1869	195.8000	91.4000	56.4000	1.6800
	2–3	8.2000×10^{-03}	5.9380×10^{-01}	8.3750×10^{-01}	5.9380×10^{-01}	1.2500×10^{-02}
	4–10	5.2000×10^{-03}	3.7190×10^{-01}	5.2500×10^{-01}	3.7190×10^{-01}	7.8000×10^{-03}
GA	1	5.1360×10^{-01}	8.4152	1.2599	2.6763	1.3820×10^{-01}
	2	2.2280×10^{-01}	14.3609	22.7735	15.0000	3.0720×10^{-01}
	3	2.3600×10^{-01}	16.4304	24.4575	15.0000	3.4540×10^{-01}
	4	2.4420×10^{-01}	2.6870	12.3826	6.6679	1.3020×10^{-01}
	5	3.9530×10^{-01}	13.0293	27.4312	15.0000	2.8820×10^{-01}
	6	1.7180×10^{-01}	10.1305	10.5638	7.8552	1.9130×10^{-01}
	7	2.0160×10^{-01}	13.8512	17.0293	11.3937	2.7560×10^{-01}
	8	4.9790×10^{-01}	24.8079	42.9948	15.0000	5.6530×10^{-01}
	9	4.9280×10^{-01}	10.9521	2.8080×10^{-01}	5.3883	8.1000×10^{-02}
	10	7.9480×10^{-01}	38.7396	64.3853	15.0000	8.5510×10^{-01}
PSO	1	1.7880×10^{-01}	11.2537	−15.7844	−15.0000	2.3200×10^{-01}
	2	8.9595×10^{-08}	5.4599×10^{-06}	-7.8945×10^{-06}	-6.3069×10^{-06}	1.0492×10^{-07}
	3	8.3187×10^{-08}	-3.6918×10^{-06}	6.0611×10^{-06}	4.7165×10^{-06}	-9.6966×10^{-08}
	4	1.7880×10^{-01}	11.2537	−15.7844	−15.0000	2.3200×10^{-01}
	5	9.9985×10^{-08}	5.8431×10^{-06}	-6.4691×10^{-06}	$-7.0337e\times10^{-06}$	1.1145×10^{-07}
	6	5.6938×10^{-08}	-3.6316×10^{-06}	3.8118×10^{-06}	2.8562×10^{-06}	-5.8678×10^{-08}
	7	8.0253×10^{-08}	-3.8333×10^{-06}	6.8407×10^{-06}	4.7161×10^{-06}	-8.4923×10^{-08}
	8	8.6374×10^{-08}	5.561×10^{-06}	-7.7736×10^{-06}	-3.8296×10^{-06}	1.1169×10^{-07}
	9	8.4415×10^{-08}	5.6505×10^{-06}	-7.6209×10^{-06}	-4.5538×10^{-06}	1.0542×10^{-08}
	10	5.8019×10^{-08}	3.5668×10^{-06}	-5.1631×10^{-06}	-2.4781×10^{-06}	7.1341×10^{-07}
NRBO	1	7.6025×10^{-08}	-4.6379×10^{-06}	4.9587×10^{-06}	3.3803×10^{-06}	-8.8197×10^{-08}
	2	7.9791×10^{-08}	5.4871×10^{-06}	-7.5024×10^{-06}	-5.0411×10^{-06}	1.1702×10^{-07}
	3	4.5000×10^{-08}	6.4174×10^{-07}	1.9462×10^{-07}	1.2416×10^{-06}	2.6760×10^{-09}
	4	7.9854×10^{-08}	4.8676×10^{-06}	-6.5382×10^{-06}	-6.4612×10^{-06}	1.0161×10^{-07}
	5	9.4780×10^{-08}	-3.5855×10^{-06}	6.8877×10^{-06}	6.4291×10^{-06}	-8.9947×10^{-08}
	6	5.4590×10^{-08}	1.4160×10^{-06}	-2.6378×10^{-06}	-2.7416×10^{-07}	4.1030×10^{-08}
	7	7.7556×10^{-08}	-3.5248×10^{-06}	4.6793×10^{-06}	5.2870×10^{-06}	-8.0933×10^{-08}
	8	9.6337×10^{-08}	2.8062×10^{-06}	-4.5705×10^{-06}	-5.1877×10^{-06}	8.0992×10^{-08}
	9	5.8400×10^{-08}	2.5450×10^{-06}	-2.3882×10^{-06}	-3.6217×10^{-06}	4.1128×10^{-08}
	10	8.9179×10^{-08}	9.6326×10^{-07}	6.7787×10^{-07}	1.6863×10^{-06}	-1.3462×10^{-08}
GNRBO	1	7.3513×10^{-08}	2.7158×10^{-06}	-4.2334×10^{-06}	-4.5209×10^{-06}	5.0032×10^{-08}
	2	9.2696×10^{-08}	8.009×10^{-07}	-1.7469×10^{-06}	-3.9857×10^{-06}	1.1163×10^{-08}
	3	6.325×10^{-08}	1.1668×10^{-06}	-1.4645×10^{-06}	-3.254×10^{-06}	3.1566×10^{-08}
	4	9.0051×10^{-08}	-1.1876×10^{-06}	-1.2955×10^{-06}	1.5039×10^{-06}	1.5501×10^{-09}
	5	7.6197×10^{-08}	-2.2943×10^{-06}	2.9585×10^{-06}	1.3215×10^{-06}	-6.004×10^{-08}
	6	9.9034×10^{-08}	2.2049×10^{-06}	-6.1565×10^{-06}	-3.8511×10^{-06}	7.6597×10^{-08}
	7	9.2146×10^{-08}	-3.2821×10^{-06}	5.5135×10^{-06}	6.2409×10^{-06}	-6.9132×10^{-08}
	8	5.795×10^{-08}	-3.2644×10^{-06}	4.9046×10^{-06}	4.1342×10^{-06}	-7.6801×10^{-08}
	9	4.4129×10^{-08}	-4.2491×10^{-06}	-2.9997×10^{-06}	-2.7219×10^{-06}	3.5641×10^{-08}
	10	5.1647×10^{-08}	2.8383×10^{-06}	-5.1605×10^{-07}	-1.2372×10^{-06}	9.7152×10^{-09}

Abbreviations: GA: Genetic Algorithm; GNRBO: Grid searching rule with an NRBO; H-J: Hooke-Jeeves algorithm; PSO: Particle Swarm Optimization; NRBO: Newton-Raphson-based optimizer.

evidenced by the residual curves, the improved algorithm demonstrates superior performance with both the smallest mean error and standard deviation in inversion results. These metrics confirm that the enhanced method achieves optimal accuracy and stability among the four compared approaches. Figure 4 presents a comparative analysis of location errors between the PSO method and the proposed method. While PSO results affected by local optima are omitted from the graph, the boxplot analysis reveals that the proposed method achieves superior convergence and stability in all three coordinate directions (X,Y,Z), with consistently lower location errors compared to PSO.

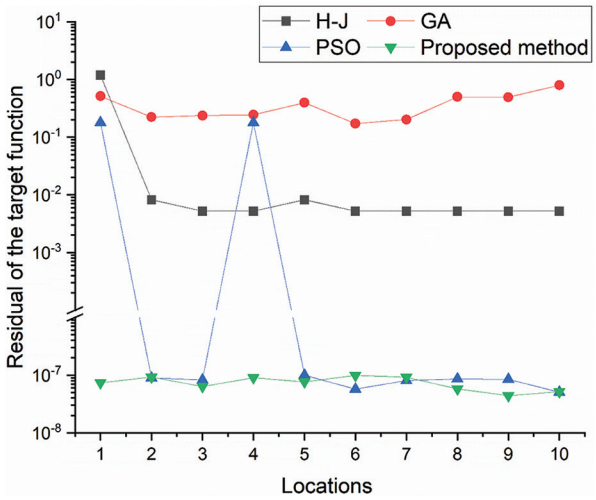

Figure 3. Residuals of the target functions of each location method for No.3 event.
Abbreviations: GA: Genetic Algorithm; H-J: Hooke-Jeeves algorithm; PSO: Particle Swarm Optimization.

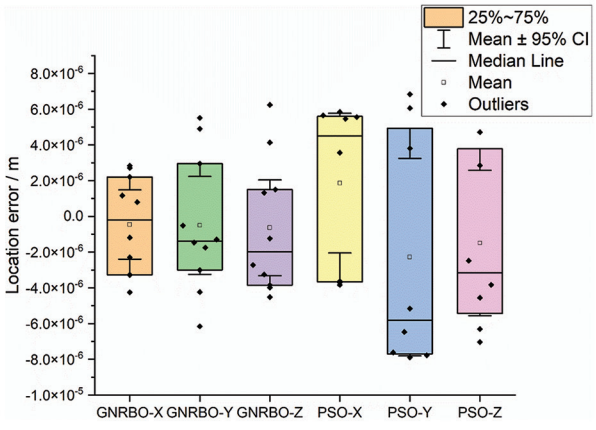

Figure 4. Location error analysis No.3 event, GNRBO-X,Y,Z are location errors on X,Y,Z directions obtained from GNRBO, PSO-X,Y,Z are location errors on X,Y,Z directions obtained from PSO function.
Abbreviations: CI: Confidence interval; GNRBO: Grid searching rule with an NRBO; PSO: Particle Swarm Optimization; NRBO: Newton–Raphson-based optimizer.

3.2. Inversion results analysis on multiple events

Using the theoretical P-wave arrival times derived from Tables 1 and 2, we applied four comparative localization methods to determine the source locations and velocity parameter for the eight microseismic events shown in Figure 3. Table 5 presents the comparative performance metrics for each method, including location errors, velocity inversion errors, and corresponding objective function values.

The results demonstrate that the H-J algorithm fails to accurately locate No.6 event, with positioning errors exceeding 50 m in both the *X* and *Z* directions. Additionally, the method yields a wave velocity error >3 mm/s.

The GA demonstrates unsatisfactory performance in both event localization and velocity inversion across all eight source events. The method fails to converge reliably to true values.

The PSO method demonstrates generally robust inversion performance, successfully converging to accurate estimates for all eight source events. However, convergence accuracy varies significantly across events, with particularly degraded performance for No.1 and 6 events compared to the other cases.

The proposed method demonstrates consistently accurate inversion results across all eight source events. The algorithm achieves unified inversion accuracy with the objective function converging to 10^{-8} magnitude. Spatial positioning errors in all three coordinate directions (X<Y, Z) converge to 10^{-7} magnitude, while velocity inversion errors stabilize at approximately magnitude.

Figure 5 presents the objective function residuals for all four methods, providing clear visual evidence of the proposed method's superior localization accuracy and stability. The residual distributions demonstrate that our approach consistently outperforms the comparison methods in both convergence precision and solution robustness.

Figure 6 presents a comparative analysis of localization errors between the PSO method and the proposed method. The boxplot visualization demonstrates superior performance of our approach in all three coordinate directions (X, Y, Z), exhibiting both enhanced convergence precision and greater solution stability compared to PSO.

4. Field data tests

To validate the practical engineering performance of the enhanced Newton–Raphson method, we conducted field verification using artificial blasting test data from a coal mine. The experimental setup included five controlled

Table 5. Location results of each algorithm for each source

Method	No.	Inversion results				
		Values of target functions	Errors on X-axis (m)	Errors on Y-axis (m)	Errors on Z-axis (m)	Velocity error (m/ms)
H-J	1	1.5800×10^{-02}	3.0125	3.1500	3.8563	1.6370×10^{-01}
	2	1.7500×10^{-02}	3.6625	1.4562	2.0937	7.2500×10^{-02}
	3	5.2000×10^{-03}	3.7190×10^{-01}	5.2500×10^{-01}	3.7190×10^{-01}	7.8000×10^{-03}
	4	1.0500×10^{-02}	1.4187	6.5000×10^{-01}	5.8750×10^{-01}	1.4400×10^{-02}
	5	3.1900×10^{-02}	2.2000	13.2375	3.7250	1.9750×10^{-01}
	6	1.2450×10^{-01}	51.5000	4.7000	54.5000	2.2200
	7	9.7000×10^{-03}	3.5000	6.3750×10^{-01}	1.3031	5.8400×10^{-02}
	8	2.1400×10^{-02}	4.0625	1.7875	9.6250×10^{-01}	6.1300×10^{-02}
GA	1	1.5100×10^{-01}	24.2526	21.5841	28.3689	1.2074
	2	2.8220×10^{-01}	15.6375	4.5920×10^{-01}	8.1980×10^{-01}	2.3230×10^{-01}
	3	1.2350×10^{-01}	8.6080	11.1370	6.5965	1.7040×10^{-01}
	4	4.4900×10^{-01}	46.0113	17.4678	22.8855	4.8210×10^{-01}
	5	2.2850×10^{-01}	8.4517	56.6445	13.4975	7.2600×10^{-01}
	6	8.8500×10^{-02}	16.3381	1.2082	20.0927	7.4680×10^{-01}
	7	2.7640×10^{-01}	108.8177	18.3472	41.8598	1.7117
	8	3.4350×10^{-01}	70.7686	28.7896	15.1159	1.0203
PSO	1	1.7831×10^{-07}	-3.3764×10^{-05}	3.5527×10^{-05}	-4.3877×10^{-05}	1.8437×10^{-06}
	2	9.2647×10^{-08}	3.7085×10^{-06}	-3.0127×10^{-06}	-5.1292×10^{-06}	-9.4259×10^{-08}
	3	8.0139×10^{-08}	-1.0875×10^{-06}	2.8362×10^{-06}	-2.2989×10^{-07}	-2.0578×10^{-08}
	4	9.3529×10^{-08}	-1.0386×10^{-05}	-4.7081×10^{-06}	6.3319×10^{-06}	1.0535×10^{-07}
	5	9.1667×10^{-08}	-6.5514×10^{-06}	-3.6093×10^{-05}	1.07×10^{-05}	5.3501×10^{-07}
	6	9.0373×10^{-06}	3.802×10^{-03}	3.8134×10^{-04}	4.005×10^{-03}	1.6129×10^{-04}
	7	9.688×10^{-08}	3.4813×10^{-05}	-6.3431×10^{-06}	-1.3297×10^{-05}	5.7872×10^{-07}
	8	9.6529×10^{-08}	-1.6689×10^{-05}	-8.0528×10^{-06}	-3.9844×10^{-06}	-2.4895×10^{-07}
GNRBO	1	4.327×10^{-08}	4.2794×10^{-06}	-3.3897×10^{-06}	5.2613×10^{-06}	-2.1536×10^{-07}
	2	9.0878×10^{-08}	-1.4828×10^{-05}	5.6007×10^{-06}	6.2505×10^{-06}	2.9693×10^{-07}
	3	9.7437×10^{-08}	-3.2897×10^{-06}	2.0745×10^{-06}	1.8301×10^{-06}	-2.9323×10^{-08}
	4	9.5457×10^{-08}	-5.2046×10^{-06}	-6.455×10^{-07}	9.316×10^{-07}	5.0079×10^{-08}
	5	6.9913×10^{-08}	-4.8094×10^{-07}	-2.5568×10^{-05}	6.3122×10^{-06}	3.8051×10^{-07}
	6	7.8638×10^{-08}	-1.9404×10^{-05}	-5.3375×10^{-07}	2.061×10^{-06}	8.487×10^{-07}
	7	6.8855×10^{-08}	6.8963×10^{-07}	-1.4791×10^{-06}	-7.0659×10^{-07}	1.2122×10^{-08}
	8	8.4659×10^{-08}	-1.1105×10^{-05}	-4.7895×10^{-06}	-3.5174×10^{-06}	-1.8259×10^{-07}

Abbreviations: GA: Genetic Algorithm; GNRBO: Grid searching rule with an NRBO; H-J: Hooke-Jeeves algorithm; PSO: Particle Swarm Optimization; NRBO: Newton-Raphson-based optimizer.

blasts, with sensor and blast locations detailed in Figure 7A and Tables 6, 7. The parameters of the GNRBO are illustrated in Table 8. Field-acquired P-wave arrival times, documented in Table 9, served as input data for the inversion. Note that neither the velocity model nor the exact origin times of the blasts were known *a priori*, reflecting realistic field conditions.

The localization results are presented in Figure 7A-D and Table 10 presents a comparative analysis of localization results between the proposed method and the coal mine's existing monitoring system. The P-wave arrival times used for both methods were selected based on signal-to-noise ratio criteria from the field data. The location results compared to the existing monitoring system, particularly in the vertical direction. Notably, the method achieves sub-10 m vertical accuracy for four out of five test events, representing a critical improvement for coal mine microseismic monitoring applications where vertical precision is paramount.

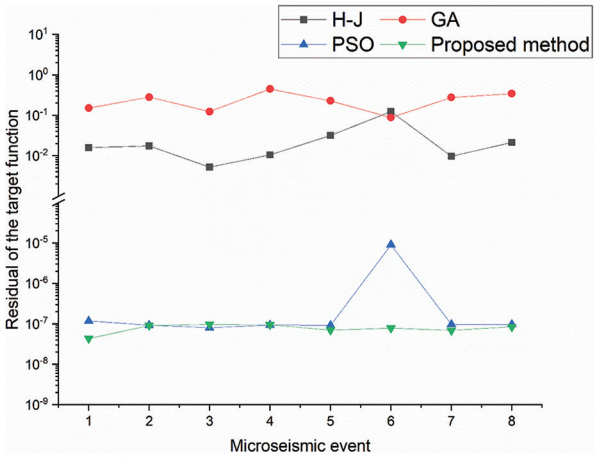

Figure 5. Residuals of the target functions of each location method for all events.
Abbreviations: GA: Genetic Algorithm; H-J: Hooke-Jeeves algorithm; PSO: Particle Swarm Optimization.

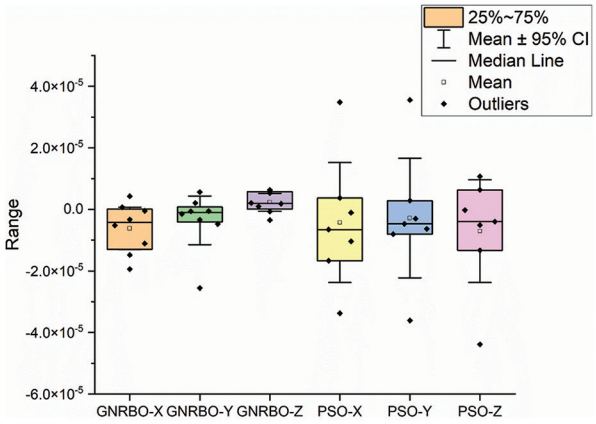

Figure 6. Location error analysis for eight events. GNRBO-X,Y,Z are location errors on X,Y,Z directions obtained from GNRBO, while PSO-X,Y,Z are location errors on X,Y,Z directions obtained from PSO.
Abbreviations: CI: Confidence interval; GNRBO: Grid searching rule with an NRBO; PSO: Particle Swarm Optimization; NRBO: Newton–Raphson-based optimizer.

5. Discussion

The current study introduces a novel approach to microseismic event location that integrates grid search principles with a Newton-Raphson-based optimizer (GNRBO). Unlike conventional arrival-time-based localization techniques, the proposed method does not require an *a priori* velocity model. Instead, it refines estimates within a four-dimensional search space (X, Y, Z, and velocity) to achieve high-precision inversion results. Given that accurate velocity parameters are often difficult to estimate or may vary during microseismic monitoring, this velocity-independent approach enhances localization accuracy.

Table 6. Coordinates of sensors in the monitoring area

Sensor	Coordinates of the sensors (m)		
	X	Y	Z
A	1490.0000	1939.3000	−870.0000
B	1416.3000	2172.4000	−887.2000
C	1350.3000	2381.5000	−890.6000
D	1519.3700	1847.5200	−866.2000
E	1767.6000	1972.2000	−900.1000
F	1699.6000	2188.7000	−908.1000
G	1623.4000	2428.4000	−915.2000
H	1685.0900	2233.5400	−904.0000
I	1467.2700	2011.5000	−878.0000
J	1399	2228.1800	−891.0000
K	1416	2170.4000	−908.5000
L	1454.9800	2050.4900	−875.7000
M	1758.3400	2001.6200	−905.0000
N	1668.1300	2287.6100	−912.0000

Table 7. True locations of microseismic events

Events	Event locations (m)		
	X	Y	Z
1	1474.1840	1984.0200	−858.0000
2	1480.6530	1955.5570	−862.0000
3	1707.8340	2139.8480	−879.0000
4	1707.2180	2129.1720	−879.0000
5	1710.8630	2130.2520	−879.0000

Existing methods, such as the original NRBO[22] and PSO, initialize search particles randomly within the solution space, which may lead to convergence at local optima rather than the global optimum—as demonstrated by the results in Table 4. In contrast, GNRBO ensures robustness by systematically generating initial iterative vectors through uniform sampling of the search space. This strategy increases the likelihood of at least one particle being sufficiently close to the global optimum, thereby improving convergence reliability.

In the synthetic data tests, we first evaluated the inversion performance for a single microseismic event. As illustrated in Figures 3-5, the proposed GNRBO method achieves significantly higher localization accuracy and greater stability compared to the three benchmark methods (H-J, GA, and PSO). While H-J and GA yield suboptimal results, PSO exhibits a tendency to converge to local optima, compromising its reliability.

Subsequently, we extended the analysis to multiple events. Figure 5 demonstrates that GNRBO successfully

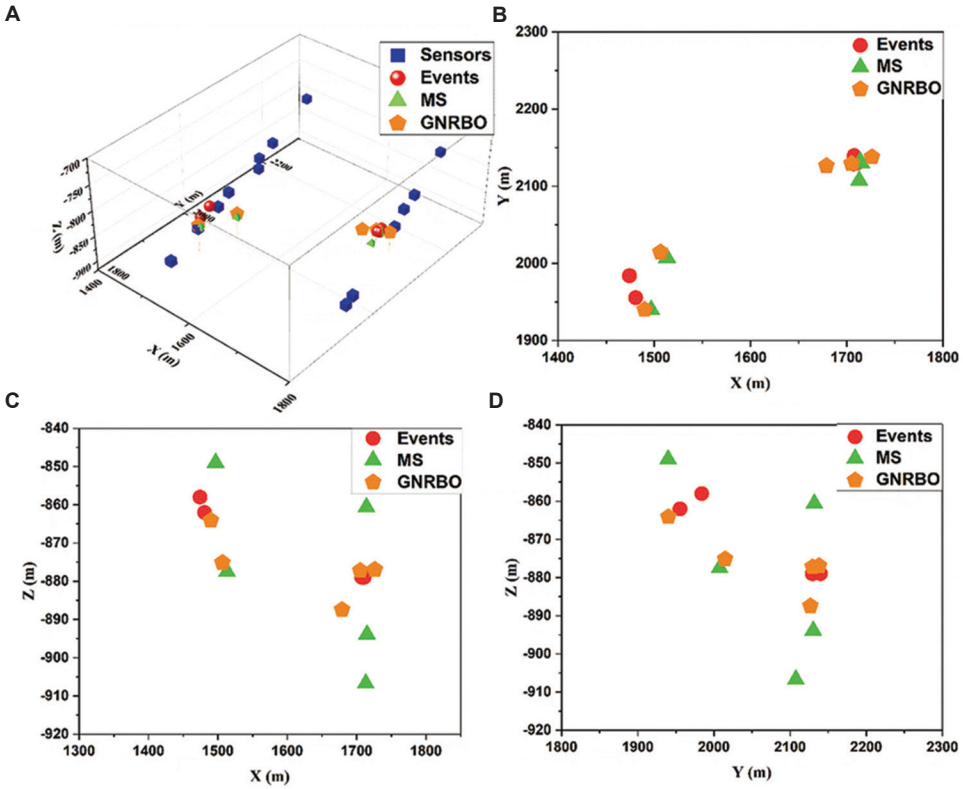

Figure 7. Microseismic monitoring in a coal mine. (A) Location results (X-Y-Z); (B) Location results (X-Y); (C) Location results (X-Z); (D) Location results (Y-Z). Abbreviations: GNRBO: Grid searching rule with an NRBO; MS: Monitoring system; NRBO: Newton–Raphson-based optimizer.

Table 8. Iteration parameters of GNRBO

Method	The range of the searching spaces				Numbers of iteration vectors	Maximum number of iterations
	X (m)	Y (m)	Z (m)	Velocity (m/ms)		
GNRBO	[1000,2000]	[1500,2500]	[−700,−1000]	[3.5]	3025 (*nx*=*ny*=11; *nz*=*nv*=5)	500

Abbreviations: GNRBO: Grid searching rule with an NRBO; NRBO: Newton-Raphson-based optimizer.

Table 9. P-wave arrival time from the field data

Sensors	Arrival times of each event (s)				
	No. 1	No. 2	No. 3	No. 4	No. 5
1	14.1120	6.0780	10.2340	9.7020	6.7560
2	14.1460	6.1340	10.2340	9.7040	6.7580
3	14.1880	/	10.2660	9.7360	6.7900
4	14.1360	6.1000	10.2460	9.7140	/
5	/	/	10.2060	/	6.7280
6	14.1560	/	10.1780	9.6500	6.7040
7	14.2000	/	10.2360	9.7080	6.7600
8	14.1600	/	10.1880	9.6600	6.7140
9	14.0960	6.0940	10.2280	9.6980	6.7520
10	14.1520	6.1440	10.2400	9.7100	6.7640
11	14.1360	6.1400	10.2280	9.6960	6.7500
12	/	/	/	/	/
13	14.1740	6.1380	/	9.6740	/
14	14.1680	6.1700	/	9.6800	6.7300

locates all eight events with high precision, outperforming the other methods. A detailed comparison of localization errors along the X, Y, and Z axes (Figure 6) further confirms the robustness of GNRBO, as evidenced by the consistently smaller error distributions in the boxplot visualization. These results conclusively demonstrate that GNRBO delivers reliable and accurate event localization in synthetic datasets, validating its superiority over benchmark method in this paper.

To evaluate the practical performance of GNRBO, we conducted field tests using artificial blasting data from a coal mine, comparing results against the mine's installed monitoring system. As demonstrated in Figure 7 and Table 10, GNRBO significantly outperforms the conventional monitoring system in localization accuracy. Detailed analysis reveals that GNRBO achieves vertical accuracy within 10 m for 80% of test events (4 out of 5), demonstrating particular improvement in vertical positioning—a critical factor for coal mine safety monitoring. These results confirm GNRBO's

Table 10. Location results based on the field datasets

Event no.	Location error (monitoring system)		Location error (GNRBO)		
	Horizontal error (m)	Vertical error (m)	Horizontal error (m)	Vertical error (m)	Sensors used
1	45.5400	19.5000	44.5300	−17.4600	A, B, C, D, F, G, H, I, J, K, M, N
2	22.4900	13.0000	17.9900	−1.5200	A, B, D, I, J, K
3	32.7700	27.7000	31.7100	−6.9900	A, B, C, D, F, G, H, I, J, K, M, N
4	7.3300	18.4000	2.1300	0.7800	A, B, C, D, F, G, H, I, J, K, M, N
5	4.2400	14.9000	17.1800	1.3500	No. 1,2,3,5,6,7,8,9,10,11,14 A, B, C, E, F, G, H, I, J, K, N

superior performance in real-world applications compared to existing monitoring solutions.

6. Conclusion

This study presents an enhanced microseismic localization and velocity inversion approach that synergistically combines grid search methodology with the Newton-Raphson algorithm. The hybrid method demonstrates significant improvements in localization accuracy and solution stability. Through comprehensive validation using both synthetic and field datasets, we comparatively evaluate our method against three established optimization techniques: the H-J algorithm, GA, and PSO. The key findings are summarized as follows:

(i) The grid search method systematically partitions the solution space to eliminate unreliable localization results caused by randomly-assigned initial vectors. By providing optimized initial parameters for the Newton-Raphson algorithm, this approach maintains high positioning accuracy while significantly improving solution stability. The grid-derived initialization vectors effectively prevent convergence to local optima.

(ii) Using synthetic data, we evaluated the inversion performance of the Newton-Raphson method in comparison with three established optimization approaches: the H-J algorithm, GA, and PSO. Through comprehensive analysis of objective function values, localization errors, and average velocity inversion errors, the results demonstrate that the proposed method achieves superior and more stable positioning accuracy.

(iii) The proposed method was validated using field data from a coal mine microseismic monitoring system. Comparative analysis with the existing localization system demonstrates superior accuracy of our approach, particularly in vertical positioning. The results reveal consistent improvements in depth estimation precision, achieving sub-10-m vertical accuracy for of seismic events (4 out of 5 test cases), which represents a critical enhancement for mine safety applications.

Acknowledgments

None.

Funding

This research was supported by the National Natural Science Foundation of China (42474189), the Open Fund Project of State Key Laboratory for Fine Exploration and Intelligent Development of Coal Research (SKLCRSM23KFA04), and the Science and Technology Innovation Team of Shandong Earthquake Agency (TD202404).

Conflict of interest

The authors declare they have no competing interests.

Author contributions

Conceptualization: Tianqi Jiang
Formal analysis: Shaohui Zhou, Yu Wang, Yajun Li
Investigation: Peng Lin
Methodology: Tianqi Jiang
Visualization: Peng Lin
Writing–original draft: Shaohui Zhou, Junhao Qu
Writing–review & editing: Shaohui Zhou

Availability of data

Data is available from the corresponding author upon reasonable request.

References

1. Ge M, Mrugala M, Iannacchione AT. Microseismic monitoring at a limestone mine. *Geotech Geol Eng.* 2009;27(3):325-339.

   doi: 10.1007/s10706-008-9234-z

2. Verdon JP, Stork AL, Kendall JM. Geomechanical modelling, microseismic monitoring and CO_2 storage. In: *EAGE/SPE Workshop on Integrated Geomechanics in Exploration and Production*. Netherlands: European Association of Geoscientists and Engineers; 2016. p. 1-5.

3. Kim K, Lees JM. Imaging volcanic infrasound sources

using time reversal mirror algorithm. *Geophys J Int*. 2015;202(3):1663-1676.

doi: 10.1093/gji/ggv237

4. Rentsch S, Buske S, Lüth S, Shapiro SA. Fast location of seismicity: A migration-type approach with application to hydraulic-fracturing data. *Geophysics*. 2007;72(1):S33-S40.

doi: 10.1190/1.2401139

5. Geiger L. Probability method for the determination of earthquake epicenters from the arrival time only. *Bull St Louis Univ*. 1912;8:60-71.

6. Li N, Wang E, Ge M, Sun Z. A nonlinear microseismic source location method based on simplex method and its residual analysis. *Arab J Geosci*. 2014;7(11):4477-4486.

doi: 10.1007/s12517-013-1121-0

7. Dong L, Li X, Zhou Z, Chen G, Ma J. Three-dimensional analytical solution of acoustic emission source location for cuboid monitoring network without premeasured wave velocity. *Trans Nonferrous Met Soc China*. 2015;25(1):293-302.

doi: 10.1016/S1003-6326(15)63604-4

8. Kushnir A, Varypaev A, Dricker I, Rozhkov M, Rozhkov N. Passive surface microseismic monitoring as a statistical problem: Location of weak microseismic signals in the presence of strongly correlated noise. *Geophys Prospect*. 2014;62(4):819-833.

doi: 10.1111/1365-2478.12124

9. Zheng J, Lu J, Jiang T, Liang Z. Microseismic event denoising via adaptive directional vector median filters. *Acta Geophys*. 2017;65(1):47-54.

doi: 10.1007/s11600-017-0005-1

10. Zheng J, Lu J, Peng S, Jiang T. An automatic microseismic or acoustic emission arrival identification scheme with deep recurrent neural networks. *Geophys J Int*. 2018;212(3):1389-1397.

doi: 10.1093/gji/ggx487

11. Li Y, Wang H, Fehler M, Fu Y. Wavefield characterization of perforation shot signals in a shale gas reservoir. *Phys Earth Planet Inter*. 2017;267:31-40.

doi: 10.1016/j.pepi.2017.04.003

12. Prange MD, Bose S, Kodio O, Djikpesse HA. An information-theoretic approach to microseismic source location. *Geophys J Int*. 2015;201(1):193-206.

doi: 10.1093/gji/ggv009

13. Jia B, Li F, Pan Y, Zhou L. Microseismic source locating method based on variable step size accelerated search. *Rock Soil Mech*. 2022;43(9):1-9.

doi: 10.16285/j.rsm.2021.5872

14. Cheng J, Song G, Liu T, Hu B, Wang J, Wang J. High precision location of micro-seismic source in underground coal mine. *Chin J Geophys*. 2016;59(2):734-743.

doi: 10.1002/cjg2.30021

15. Gong S, Dou L, Ma X, Liu J. The method to identify the optimal channel numbers for increasing the location accuracy of microseismic events in coal mine. *J China Coal Soc*. 2010;35(12):2017-2021.

doi: 10.13225/j.cnki.jccs.2010.12.014

16. Gong S, Dou L, Ma X, Mu Z, Lu C. Optimization algorithm of network configuration for improving location accuracy of microseism in coal mine. *Chin J Rock Mech Eng*. 2012;31(1):8-17.

17. Duncan PM, Eisner L. Reservoir characterization using surface microseismic monitoring. *Geophysics*. 2010;75(5):139-146.

doi: 10.1190/1.3467760

18. Jiang T, Pei S. Micro-seismic event location based on Newton iteration method and grid-search method. *J Min Sci Technol*. 2019;4(6):480-488.

doi: 10.19606/j.cnki.jmst.2019.06.002

19. Lü J, Jiang Y, Zhao Y, Zhu J, Wang X, Tao L. Study of microseismic positioning based on steady simulated annealing-simplex hybrid algorithm. *Rock Soil Mech*. 2013;34(8):2195-2203.

doi: 10.16285/j.rsm.2013.08.024

20. Luo H, Yu J, Pan Y, Song B, Liu L, Liang J. Seagull optimization based on quantile difference mine earthquake location method. *Prog Geophys*. 2022;37(1):421-429.

doi: 10.6038/pg2022FF0401

21. Dong L, Li X, Tang L, Gong F. Mathematical functions and parameters for microseismic source location without pre-measuring speed. *Chin J Rock Mech Eng*. 2011;30(10):2057-2067.

22. Sowmya R, Premkumar M, Jangir P. Newton-Raphson-based optimizer: A new population-based metaheuristic algorithm for continuous optimization problems. *Eng Appl Artif Intell*. 2024;128:107532.

doi: 10.1016/j.engappai.2023.107532